Journal of Materials Chemistry C

Accepted Manuscript

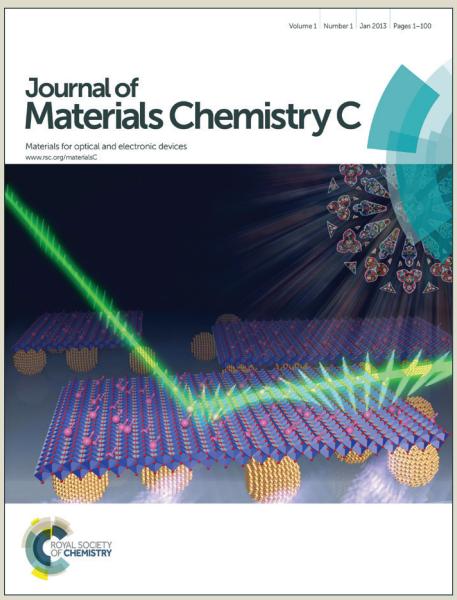

ROYAL SOCIETY OF CHEMISTRY

www.rsc.org/materialsC

CO catalytic oxidation on Al-doped graphene-like ZnO monolayer sheets: a first-principles study

Dongwei Ma[1,*], Qinggao Wang[1], Tingxian Li[1], Zhenjie Tang[1], Gui Yang[1], Chaozheng He[2,*], and Zhansheng Lu[3]

[1]*School of Physics, Anyang Normal University, Anyang 455000, China*

[2]*Physics and Electronic Engineering College, Nanyang Normal University, Nanyang 473061, China*

[3] *College of Physics and Electronic Engineering, Henan Normal University, Xinxiang 453007, China*

Abstract

The graphene-like ZnO (g-ZnO) monolayer sheet is a new class of two-dimensional materials with unique properties, which are still largely unexplored. This work studied the modulation of electronic structures and chemical activities of the g-ZnO monolayer sheet by substituting Al for host Zn atoms. It is found that replacing Zn with Al atoms is both energetically and dynamically highly favorable. Al doping introduces electrons into the conduction band of the g-ZnO monolayer sheet, which should significantly enhance the conductance and the chemical activity of the sheet. The CO oxidation by the lattice O atoms via the Mars-van Krevelen mechanism, and by the adsorbed O_2 via the Langmuir-Hinshelwood and Eley-Rideal mechanisms were comparably studied. The Al-doped g-ZnO monolayer sheet shows good catalytic activity for the CO oxidation via the more favorable Eley-Rideal mechanism with a two-step route. The study presents an effective strategy to tune the electronic structure and the chemical activity of the g-ZnO nanosheets, and gives us an insight into the mechanism of Al-doped ZnO nanostructures sensing reducing gases.

Keywords:

Graphene-like ZnO, Al doping, CO oxidation, First-principles calculation

*Corresponding author. E-mail: dwmachina@126.com (Dongwei Ma).
*Corresponding author. E-mail: hecz2013@nynu.edu.cn (Chaozheng He).

1, Introduction

ZnO is a II-VI compound semiconductor with a wide direct band gap of 3.37 eV at room temperature and a large exciton binding energy of 60 meV, which makes ZnO having great potential for a variety of practical applications, such as field-effect transistors, photodetectors, photocatalysts, transparent conductive oxides, solar cells and gas sensors.[1-7] As a result, there is considerable interest in studying ZnO in the forms of powders, single crystals, thin films, or nanostructures. ZnO nanostructures with various morphologies, such as nanowires,[8, 9] nanorods,[10, 11] nanoflowers,[12, 13] nanoribbons,[14, 15] and nanotubes,[16, 17] have been successfully synthesized for tuning their functionalities.

Interestingly, graphene-like ZnO (g-ZnO) nanosheets can also exist and exhibit unique properties.[18-23] The two-dimensional (2D) g-ZnO monolayer sheet with a honeycomb lattice was first predicted theoretically to be analogue of h-BN, where B and N atoms are replaced by Zn and O, respectively.[18] The flat, layered 2D ZnO nanosheets was then observed in experiments.[20-22] The successful synthesis of g-ZnO nanosheets in experiments have aroused enormous theoretical interest in this 2D material.[23-35] For example, Topsakal et al. studied theoretically the atomic, electronic, and magnetic properties of 2D, single and bilayer g-ZnO sheets and their armchair and zigzag nanoribbons.[23] Schmidt et al. demonstrated theoretically that Co doped g-ZnO monolayer sheets present ferromagnetic coupling.[24] Wang et al. investigated the structural, electronic, and magnetic properties of the fully fluorinated and semifluorinated g-ZnO monolayer sheets.[25] Tang et al. found in g-ZnO nanosheets the semiconductor → half-metal → metal transition occurs with nonmagnetic → magnetic transfer upon adopting surface hydrogenation and increasing sheet thickness.[26] In addition, replacing lattice O by C, N, or B atoms can also make g-ZnO monolayer sheets to exhibit a nonmagnetic → antiferromagnetic → ferromagnetic transition.[27]

However, up to date, most availabe theoretical researches on g-ZnO nanosheets mainly foucs on the modulation of their electronic and magnetic properties. There are few studies on the change of surface chemical properties of g-ZnO nanosheets

induced by the means, such as doping, strain and external fields. In this aspect, very recently Zhang et al. theoretically studied the CO adsorption and the induced change in the electronic and magnetic properties of g-ZnO monolayer sheets doped with B, N, or C.[36] Kouser et al. demonstrated that g-ZnO monolayer sheets doped with N are promising materials to facilitate capturing of toxic H_2S and at the same time converting it to a green source of energy.[37] Zhang et al. using first-principles calculations showed that g-ZnO monolayer sheets are good substrates for Au_8 clusters catalyzing CO oxdiation reaction, which provides new opportunities for the future development of ZnO-based catalysts.[38] On the other hand, in the past several years a lot of theoretical studies have shown that substitutional doping is an effective strategy for improving the surface chemical activity of 2D materials, such as graphene and h-BN.[39-44] The improved surface chemical activity makes these 2D materials having great potential in the fields of catalysis and sensing. For example, Feng et al. using first-principles calculations displayed that filling the C monovacancy with a Au atom in graphene makes it a highly active CO oxidation catalyst with the highest energy barrier as low as 0.31 eV.[39] They also investigated theoretically the adsorption of small gas molecules on various transition-metal doped graphene and suggested the doped graphene as a potential material for gas sensing and catalysis applications.[42]

Inspired by the above findings, using first-principles calculations, herein we studied the effect of substituting Al for Zn atoms on the electronic structure of the g-ZnO monolayer sheet, and the adsorption of CO and O_2 as well as the oxidation of CO on the sheet. The element Al has been selected as the dopant due to that recently several experimental studies demonstrated that Al doping can significantly enhance the response of ZnO nanostructures at a lower temperature compared with the undoped counterparts towards reducing gases, such as CO[45-48] and ethanol,[47, 49-51] for which the underlying mechanism is still unclear. For the Al-doped ZnO nanostructures, it is easy for Zn^{2+} in the ZnO lattice to be replaced by Al^{3+}, due to the smaller ionic radius of Al^{3+} (0.057 Å) than that of Zn^{2+} (0.074 Å). The CO oxidation reaction has been investigated, as CO is one of the poisonous and harmful gases in the air, and its sensing and removing are considred to be highly important for the envioremental safty

and human health.[52] Our calculations suggest that Al-doped g-ZnO (Al-g-ZnO) monolayer sheets are promising catalysts for CO oxidation and sensitive CO sensors operating at low temperature.

2, Computational methods

All the calculations were performed with the projected augmented wave (PAW) formalism of density functional theory (DFT), as implemented in the Vienna Ab-initio Simulation Package (VASP).[53-55] The generalized gradient approximation (GGA) method with Perdew-Burke-Ernzerhof (PBE) for the exchange-correlation energy was used.[56] The cutoff energy for the planewave basis set was taken as 400 eV. A 5 × 5 supercell of the g-ZnO monolayer sheet (Fig. 1(a)) was used and the distance between the sheet and its neighboring image is about 16 Å. Correspondingly, the Brillouin zone integrations were performed by using a Monkhorst-Pack (MP) grid of 2 × 2 × 1.[57] The convergence of the total energy was considered to be achieved until two iterated steps with energy difference less than 10^{-5} eV. Structural optimization was performed until the Hellmann-Feynman force on each atom was less than 0.02 eV/Å. During the optimization, all the internal coordinates were allowed to relax with a fixed lattice parameter. All the calculations were performed with spin-polarization and a MP grid of 4 × 4 × 1 was used for the calculations of the densities of states (DOS).

The climbing image nudged elastic band method (CI-NEB)[58] was used to find the minimum-energy path (MEP). Four to eight images were inserted in between two stable states, and the spring force between adjacent images was 5.0 eV/Å. The geometric optimization and the search for the transition state (TS) were tested by means of frequency calculations.

3. Results and discussion

3.1 The g-ZnO and Al-g-ZnO monolayer sheets

The initial strcuture of the g-ZnO monolayer sheet is cut from a bulk wurtzite ZnO(0001) polar surface, consistant with the structure of the g-ZnO monolayer sheet synthesized experimentally.[20-22] The optimized structure of the g-ZnO monolayer sheet is a graphene-like flat sheet. The calculated lattice paramter of the primitive cell

is 3.286 Å with the Zn-O bond length of ~ 1.90 Å, which agrees well with the experimental value of 1.92 Å[20] and previously GGA values of 1.90 Å.[23, 38] The atomic configuration and the DOS for the 5 × 5 supercell of the g-ZnO monolayer sheet are shown in Figs. 1(a) and 1(b), respectively, where the position of the replaced Zn atom (or the dopant) is indicated by the blue circle. The calculated band gap of 1.51 eV is in good agreement with the previous theoretical resutls.[23, 37] As shown in Fig. 1(b), the valence band of the g-ZnO monolayer sheet can be divided into two regions: the lower part from about -6.8 to -4.6 eV and the upper part from about -4.6 to -0.3 eV, of which the lower valence band is mainly contributed by Zn 3*d* states, while the upper part comes mainly from O 2*p* states. In addition, the conduction band of the g-ZnO monolayer sheet is mainly composed of O 2*p* and Zn 4*s* states. This electronic structure characteristic is in good agreement with that presented in Ref.[37].

The atomic configurations for the Al-g-ZnO monolayer sheet are shown in Fig. 2(a). The bond lengths between the dopant Al and its three nearest O are all 1.74 Å, which is smallar than the Zn-O bond length (1.90 Å) of the pristine g-ZnO monolayer sheet. This will induce strain into the lattice of the g-ZnO monolayer sheet, while the dopant Al atom is still at the same plane as the Zn and O atoms. It is expected that the *n*-type conductivity can be achieved through replacing a Zn with an Al atoms for the g-ZnO monolayer sheet. The Bader charge ananlysis[59] shows that the amount of valence electrons of the Al dopant is 0.69 *e*, which is close to the calculated one of 0.55 *e* for bulk α-Al_2O_3. Therefore, the dopant Al can be considered to be +3 oxidation state and it is an effective donor for the g-ZnO monolayer sheet. The DOS analysis further confirms this point, which are shown in Fig. 2(b). The total DOS (TDOS) of g-ZnO and Al-g-ZnO monolayer sheets are shown in the upper panel of Fig. 2(b), from which it can be seen that the Fermi level of the Al-g-ZnO monolayer sheet shifts upward into the conduction band compared with the undoped counterpart. Thus, the electrons released by the doped Al are introduced into the conduction band of the g-ZnO monolayer sheet, which increases the concentration of free electrons, resulting in the decrease in the resistance of the sheet. The local DOS (LDOS) projected on the Al dopant are shown in the lower panel of Fig. 2(b) and they only

make a very small contribution to the states just below the Fermi level. Furthmore, the electron density distributions for the Al-g-ZnO monolayer sheet within the energy interval from -0.5 to 0 eV with respect to the Fermi level are shown in Fig. 2(a). We can see that these states spread over the whole supercell, which indicates the metallic behaviors of the doped systems.

To examine the feasibility of the formation of the Al-g-ZnO monolayer sheet, we calculated its formation energy, which is defined as: $E_{\text{form}} = (E(\text{Al-g-ZnO}) + \mu(\text{Zn})) - (E(\text{g-ZnO}) + \mu(\text{Al}))$, where E(Al-g-ZnO) and E(g-ZnO) are the total energies of the Al-g-ZnO and g-ZnO monolayer sheets, respectively, and μ(Zn) and μ(Al) are the chemical potentials for Zn and Al, respectively. μ(Zn) and μ(Al) are taken as the cohesive energy per atom of hcp Zn and fcc Al, respectively. The similar definitions for the formation energy have been used previously.[60, 61] By this definition, a negative formation energy indicates that it is energetically favorable to replace a Zn atom with an Al dopant. The calculated formation energy of -1.18 eV suggests that it is highly energetically feasible for the formation of the Al-doped g-ZnO monolayer sheet. We also studied the adsorption of the Al single atom on the surface of the pristine g-ZnO monolayer sheet, for which the adsorption energy has been defined with respect to the isolated Al atom and the free-standing g-ZnO monolayer sheet. As shown in Fig. 3, the Al atom can be anchored on top of a O atom (Fig. 3(a)) or the hollow site above a Zn-O hexagonal ring ((Fig. 3(b))) with the adsorption energies of 1.79 and 2.05 eV, respectively. These energies are much smaller than the released energy (11.04 eV) for filling an Al dopant into a Zn vacancy of the g-ZnO monolayer sheet. The above results strongly suggest that it is energetically favorable for the formation of the Al-g-ZnO monolayer sheet. The Al atom can also locates on top of a Zn atom with the adsorption energy of 0.60 eV and the Al-Zn distance of 2.69 Å (Fig. 3(c)). Interestingly, from the initial configutaion with a short Al-Zn distance of ~ 1.7 Å, the configuraion of the Al-g-ZnO monolayer sheet with a weakly adsorbed Zn atom can be obtained after the geometric optimization (Fig. 3(d)). We have calculated the MEP for the transition from the state shown in Fig. 3(c) to that shwon in Fig. 3(d). It is found that the process is barrierless for the Al atom pushing out of the Zn atom and

entering into the Zn site, which indicates that the synthesis of the Al-g-ZnO nanosheets may be realized by directly depositing Al atoms on the g-ZnO nanosheets.

3.2 Adsorption of O_2 and CO on the Al-g-ZnO monolayer sheet

From the above, we can see that Al doping leads to the upshit of the Fermi level into the conduction band of the g-ZnO monolayer sheet, which will lower the work function of the system. The calculated work function for the g-ZnO and Al-g-ZnO monolayer sheets are 4.72 and 3.18 eV, respectively. The decrease in the work function will facilitate the release of electrons from the surface to adsorbed species, thus enhancing the interaction between them.[62]

As a reference, the calculation results of the adsorption of O_2 and CO molecules on the pristine g-ZnO monolayer sheet were presented firstly. To evaluate the stability of the molecules on the g-ZnO monolayer sheet, the adsorption energy of the adsorbates was defined as: $E_a(\text{ads}) = E(\text{g-ZnO}) + E(\text{ads}) - E(\text{ads/g-ZnO})$, where E(ads), E(g-ZnO), and E(ads/g-ZnO) are total energies of the free adsorbate, the pristine g-ZnO monolayer sheet and the sheet with the adsorbate, respectively. The similar definition has been used for the adsorption of O_2 and CO molecules on the Al-g-ZnO monolayer sheet. Various initial configurations have been considered in order to find the most stable one for each adsorbate. After full relaxation, as shown in Fig. S1, the nearest distance between the adsorbed O_2 or CO molecules and the g-ZnO monolayer sheet is very large of about 3 Å, which indicates the physisoption of the molecules. The calculated adsorption energies for both O_2 and CO are in the order of 0.01 eV, further confirming the weak interaction between the adsorbates and the sheets.

As expected, the adsorption of O_2 and CO molecules on the Al-g-ZnO monolayer sheet is much stronger than that on the g-ZnO monolayer sheet. For the adsorption of O_2 and CO molecules on the Al-g-ZnO monolayer sheet, we have considered not only the sites around the dopant Al atom, but also those away from it. As a result, we found that O_2 can interact strongly with the Al-g-ZnO monolayer sheet even if the adsorption sites are far away from the doped Al atom. Two such configuraions for the O_2 adsorption are shown in Fig. S2, which have the adsorption energies of ~ 1 eV.

However, CO can only be physisorbed on the sites away from the doped Al atom. The different adsorption behevior for O_2 and CO may result from that O_2 has lower $2\pi^*$ anti-bonding orbitals with respect to the Fermi level than CO and thus it is easier for O_2 than CO to gain electrons from the sheet.

The parameters of the obtained most stable configuraions for the adsorption of O_2 and CO on the Al-g-ZnO monolayer sheet are displayed in Table 1. As shown in Fig. 4(a), the most stable configuration for the O_2 adsorption has the molecule bridging the doped Al and one of its nearest Zn atoms. This configuration with the adsorption energy of 2.30 eV is much more stable than those displayed in Fig. S2. The possible reason for this is as follows. The enhanced binding of O_2 on the Al-g-ZnO monolayer sheet on the sites away from the doped Al just benefits from the reducd work function compared with the g-ZnO monolayer sheet. However, the enhanced binding of O_2 on the Al-g-ZnO monolayer sheet near the doped Al benifits not only from the reduced work function but also the potential higher coordination of doped Al in oxides than Zn, which make doped Al prone to adsorb O_2 from the gas phase to satisfy its higher coordination. For example, Zn atoms in wurtzite ZnO are 4-fold coordinated, while Al atoms in α-Al_2O_3 6-fold coordinated.

The strong interaction between the adsorbed O_2 and the Al-g-ZnO monolayer sheet involves the formation of short bonds between the adsorbate and the sheet. As shown in Fig. 4a, the length of the formed Zn-O1 bond is 2.24 Å, and that of the Al-O2 bond 1.90 Å. The O-O bond length of the adsorbed O_2 is elongated to 1.39 Å, which is close to that of the free O_2^- (1.36 Å) and much larger than that of the free O_2 molecule (1.29 Å). The elongation of the O-O bond can be probably explained by the result of Bader charge analysis.[59] It is found that there is -0.83 *e* charge transfer from the sheet to the adsorbed O_2, which fills the anti-bonding $2\pi^*$ orbitals of the O_2, as shown in Figs. 4(b) and (c). As shown in Fig. 2(b), the dopant Al makes very small contribution to the electron states just below the Fermi level, correspondingly there is very few charge (-0.10 *e*) transfer from the Al to the adsorbed O_2. The charge transfer reduces the spin magnetic moment of the O_2 to 0.98 μ_B. In addtion, the stretching frequency (1178.0 cm^{-1}) of the adsorbed O_2 is close to that (1253.1 cm-1) of the free

O_2^-. Therefore, according to above, the adsorbed O_2 can be assigned to superoxo O_2^-, which is active to catalyze oxidation of reducing molecules.

The DOS analyses for the configuration shown in Fig. 4(a) were performed. As shown in the upper panel of Fig. 4(b), large tranfer of electrons from the sheet to the adsorbed O_2 shfits down the fermi level close to the valence band, and as a result, the TDOS are similar to those of the pristine g-ZnO monolayer sheet (Fig. 2(b)), except that there are some impurity states from the adsorbed O_2 just above the Fermi level. Therefore, the adsorption of O_2 molecules should significantly decrease the conductance of the Al-g-ZnO monolayer sheet. From the LDOS (the lower panel of Fig. 4(b)), we can see that the spin-down states of the $2\pi^*$ anti-bonding orbital of the adsorbed O_2 are split and half-filled, which is in line with the Bader charge analysis. This can be further confirmed by the electron density distributions shown in Fig. 4(c) within the energy interval from -0.5 to 0 eV with respect to the Fermi level. In addition, the 1π states show strong resonance with the states of the Al and Zn atoms bonded with the adsorbed O_2, suggesting the partial covalent characteristics of the interaction between the adsorbate and the sheet.

In addtion, some configurations for the O_2 dissociative adsorption have been investigated and the obtained stable ones are shown in Fig. S(3). The calculated adsorption energy with respect to the free O_2 molecule and the bare Al-g-ZnO sheet shows that all the systems are only slightly exothermic with the largest adsorption energy of only 0.24 eV. Obviously, the molecular adsorption state (as shown in Fig. 4(a)) with an adsorption energy of 2.30 eV is much more stable than the dissociative adsorption states. This energy difference suggests that the dissociation of the adsorbed O_2 to atomic O are highly endothermic and energetically unfavorable, and has to overcome a barrier of at least 2 eV. Especially, this value is much higher than the highest energy barrier of 0.79 eV for the CO oxidation via the most favorable mechanism (as discussed below). Therefore, CO oxidation by the adsorbed O atom formed by the dissociation of the adsorbed O_2 molecule has not been further investigated in this work.

Contrary to O_2, the interaction between CO and the Al-g-ZnO monolayer sheet is

much weaker. As shown in Fig. 5(a), the most stable configuration with the adsorption energy of 0.47 eV has the C end binding with the doped Al atom and the C-O bond almost perpendicular to the Al-g-ZnO monolayer sheet. The interaction with the sheet slightly increases the length of the C-O bond by ~ 0.02 to 1.18 Å, which may result from the transfer of electrons from the sheet to the anti-bonding $2\pi^*$ orbitals of the adsorbed CO. Bader charge analyses show that the CO molecule has gained charge of -0.37 *e*, among which only -0.07 *e* comes from the doped Al atom. In addition, the charge tranfer induces spin magnetic moment in the adsorbed CO (0.42 μ_B) and the sheet (0.07μ_B). The DOS analyses for the configuration shown in Fig. 5(a) were performed. Compared with the TDOS (Fig. 2(b)) of the Al-g-ZnO monolayer sheet, the tranfer of electrons from the sheet to the adsorbed CO slightly shifts down the Fermi level (the upper panel of Fig. 5(b)). Therefore, the CO adsorption should also decrease the conductance of the Al-g-ZnO monolayer sheet. From the LDOS (the lower panel of Fig. 5(b)), it can be seen that the spin-up states of the $2\pi^*$ anti-bonding orbital of the CO are slighly filled due to the transfer of electrons, which are high above the Fermi level for the free CO. In addition, there is no significant resonance between the states of the CO and its bonded Al atom, thus the interaction between CO and the sheet is maily ionic.

3.3 CO oxidation on the Al-g-ZnO monolayer sheet

Most heterogenuous oxidation reactions catalyzed by metal oxides take place via the Mars-van Krevelen (MvK) mechanism, in which the reductant molecules react with oxygen atoms from the surface of metal oxides.[63-67] The oxidized molecules desorb and take oxygen with them, leaving hehind oxygen vacancies on the surface. These vacancies are filled by one O atom of the O_2 molecules from the gas phase and another O atom will further oxidze a reactant molecule from the gas phase. Finally, after the desorption of the oxidized molecules the oxygen vacancies are filled by the remaining O atom and the catalytic cycle are completed. Given this, the CO oxidation via the MvK mechanism was firstly considered. However, we find that the processes of CO oxidation via this mechanism to produce CO_2 (CO + Al-g-ZnO → CO_2 + Al-g-ZnO_{1-x}) are endothermic by 0.36 to 1.76 eV depending on the position of the O

sites with respect to the doped Al, which indicates that the processes are energetically unfavorable.

Another two well-estabilshed mechanisms for the CO oxidation are the Langmuir-Hinshelwood (LH) and Eley-Rideal (ER) mechanisms, which have been widely investigated on meal surfaces, metal clusters, or metal single atoms embeded in the low-dimensional materials.[39, 68-71] For the ER mechanism, the gas-phase CO molecules directly react with the preadsorbed O_2 molecules, producing a carbonate-like CO_3 complex as intermediate state (MS). The LH mechanism involes the coadsorption of CO and O_2 molecules before reaction, the formation of a peroxo-type OOCO complex MS and the desoprtion of the produced CO_2 molecules. Below, both mechanisms were investigated comparably.

Several coadsorption configurations via the LH mechanism were tested. Initially, O_2 and CO molecules were put at rather close. However, no stable CO_2 or OOCO MS formation was found after full optimization (as shown in Fig. S4). In Fig. S4(a), it is obvious that although initially CO and O_2 molecules bonded with the active Al atom are close to each other, while after full optimization the CO molecule desorbs from the substrate and the distance between the CO and the adsorbed O_2 is larger than 3 Å. In Fig. S4(b), initially CO and O_2 molecules are also coadsorbed on the active Al atom, while after full optimization only C atom is bonded with the Al atom of the substrate. Especially, the formation of this state is endothermic by 0.28 eV with respect to the free CO molecule and the O_2-covered Al-g-ZnO, which indicates that the process is energetically unfavorable. This indicates that the reaction process of CO oxidation on the Al-g-ZnO monolayer sheet via the LH mechanism is almost impossible or proceeds with great difficulty. This conclusion is further enhanced when we consider the much more favorable adsorption of O_2 than CO. Similarly, Li et al. found that CO oxidation on the Fe-embedded graphene can not be initiated via the LH mechanism.[40] Therefore, in the following we focus on the ER mechanism.

The atomic configurations of each state along the reaction path initiated via the ER mechanism are displayed in Fig. 6, and the corresponding energy profiles are summarized in Fig. 7. The configuration of physisorbed CO above O_2 preadsorbed on

the Al-g-ZnO monolayer sheet was selected as the initial state (IS, Fig. 6(a)). When approaching the activated O_2, one CO molecule can be inserted into the O-O bond to form a carbonate-like complex (MS1, Fig. 6(c)) bridging the doped Al and one of its nearest Zn atoms, where the O-O bond length is further elongated to 2.30 Å. This is quite similar to the reaction of CO on the Fe-embedded graphene.[40] The process of CO insertion into the O-O bond is exothermic by 3.93 eV and only a very small barrier of 0.06 eV should be overcome (Fig. 7), which involves the rotation of the O1-O2 bond above the Zn-O hexagonal ring. One may expect that when the CO molecule approaching the O_2-covered Al-g-ZnO monolayer sheet to form the carbonate-like CO_3 complex, the bond of the adsorbed O_2 molecule will be further elongated to accommodate the incoming CO molecule. Thus, in the TS1 the O1 and O2 atoms will be still bonded with the Zn and the dopant Al atoms, respectively, as in the IS and MS1. However, our calculation shows that if O1 and O2 atoms are initially put on top of the Zn and Al atoms, respectively, after optimization two O atoms are recombined as the adsorbed O_2 molecule. This suggests that further elongation of the O1-O2 bond of the adsorbed O_2 should be highly energetically unfavorable. To form the carbonate-like CO_3 complex, the CO and adsorbed O_2 molecules should firstly approach to each other. In fact, the CI-NEB calculations show that for this end the CO and the adsorbed O_2 rotate simultaneously with respect to the substrate, may due to the attraction interaction of the negatively charged O1 and the positively charged C atoms. It is the rotation of the O_2 molecule that leads to the break of the Zn-O1 bonds and the formation of the Al-O1 bond in the TS1. As a result, in the TS1 both O1 and O2 atoms are bonded with the dopant Al atom.

Next, the carbonate-like complex in MS1 may directly dissociate to produce a physisorbed CO_2 on the Al-g-ZnO monolayer sheet with an adsorbed atomic O. However, as shown in Fig. S5, such state is less stable than MS1 by 1.48 eV. Therefore, the direct dissociation of the carbonate-like complex in MS1 to produce a CO_2 molecule needs to overcome a barrier of at least 1.48 eV, and consequently this process are unfavorable both energetically and dynamically. Then we considered another reaction path involving the process that MS1 reacts with another CO molecule

to produce two CO_2 molecules. Initially, the second CO molecule locates on top of one Zn atom near the doped Al atom (MS2, Fig.6(d)). The distance between the second CO and its bonded Zn atom (C2-Zn) as well as the carbonate-like complex (C2-O2) are 2.47 and 3.50 Å, respectively. Reaching TS2 (Fig 6(e)), C2-Zn and C2-O2 distances reduce to 2.17 and 1.70 Å , respectively. However, the C1-O2 bond length elongates from 1.32 Å in the MS2 to 1.49 Å in the TS2, which is crucial to the formation of the two CO_2 molecules. Passing over TS2 with an energy barrier of 0.79 eV, two CO_2 molecules are produced (Fig. 6(f)) with the adsorption energy of 0.46 eV with respect to two free CO_2 molecules in the gas phase. Since the energy released in this step (0.79 eV) can sufficiently surmount the adsorption energy, these two CO_2 molecules can be released rather easily from the FS.

Overall, the highest barrier is 0.79 eV for the CO oxidation on the Al-g-ZnO monolayer sheet along the whole MEP. This value is higher than those predicted for the CO oxidation on the other 2D materials with embedded metal atoms, such as Au-graphene (0.31 eV),[39] Fe-graphene (0.58 eV),[40] Cu-graphene (0.54 eV),[41]Co-h-BN (0.52 eV),[43] and Au-h-BN (0.47 eV).[44] However, it is low enough for the reaction to proceed rapidly at low temperature (the typical time scale for this reaction at 350 K (300 K) is about 0.01 s (1s) with a prefactor of 10^{13} s^{-1}),[72, 73] suggesting that the Al-g-ZnO monolayer sheet would be an efficient catalyst for CO oxdiation at low temperature. The strong adsorption and significant activation of O_2 on the Al-g-ZnO monolayer sheet also indicate that the sheet may be good catalysts catalysing other oxidation reactions, such as NO oxidation.[74] It is interesting to perform a real-time demonstration of the CO oxidation reaction investigated at the present work , which may be realized by the *ab initio* molecular dynamics (AIMD) simulations.[75] Usually, the time step for a AIMD simulation is on the order of fs (10^{-15} s). Accordingly, current computer resources only allow a reaction happening one time within about 100 ps (10^{-10} s) to be observed. The timescale (0.01 s or 1s) estimated for the CO oxidation reaction at the present work is much larger than that of 10^{-10} s, and thus the real-time demonstration of this reaction is not possible presently, due to the limitation of the computer resource.

In addtion, recent experiments have shown that Al doping can increase the conductivity of the ZnO nanostructures and enhance their response twoards CO in air at the operating temperature of far above room temperature (300K).[45-48] Our results indicate that the Al-g-ZnO monolayer sheet may be a sensitive CO sensor at room temperature thanks to the modest energy barrier (0.79 eV) for completing the CO oxidation reaction. The sensing mechanism of the Al-g-ZnO monolayer sheet towards CO can be explained as follows. Upon Al doping, electrons are introduced into the conduction band of the g-ZnO monolayer sheet (Fig. 2), which increases the concentration of free electrons, resulting in the decrase in the resistance of the sheet. When the sample is exposed to air, oxygen molecules in the air capture electrons from the doped sheet (Fig. 4), resulting in the increase in the resistance of the sheet. After the desorption of the produced two CO_2, the catalytic cycle is completed and the electrons captured by the adsorbed O_2 are reinjected into the conduction band of the g-ZnO monolayer sheet. Consequently, our study provides an effective stragetgy to convert the inert g-ZnO sheet through introduction of dopant to chemically active one, facilitating its applications in the fields of catalysis and sensing. In addition, present study will give us an insight into the the mechanism of Al-doped ZnO nanostructures sensing reducing gases, such as CO[45-48] and ethanol.[47, 49-51]

4. Conclusions

In summary, we have investigated the electronic structure, structural stability, and catalytic activity of the Al-g-ZnO monolayer sheet. It is found that the process of replacing a Zn atom with an Al atom is highly exothermic and Al atoms can barrierlessly push out of Zn atoms and enter into the Zn sites. Upon doping, electrons are introduced into the conduction band of the g-ZnO monolayer sheet, which should significantly enhance the conductance and the chemical activity of the sheet. O_2 can be strongly adsorbed and activited on the Al-g-ZnO monolayer sheet with an adsorption energy of 2.30 eV. The oxidation of CO were studied comparably via three mechanisms, i.e., the MvK mechanism by the lattice O atoms, the LH and ER mechanisms by the activated O_2. As a result, the CO oxidation via the former two mechanisms would be energetically and dynamically unfavorable. The CO oxidation

via the ER mechanism is started by forming a carbonate-like CO_3 with a very small energy barrier of 0.06 eV. Then the CO_3 reacts with another CO to produce two CO_2 molecules with a larger barrier of 0.79 eV. Our results demonstrate that the Al-g-ZnO monolayer sheets are promising materials for CO oxidation and sensing at low temperature. This study provides an effective stragetgy to tune the electronic structure and the chemical activity of the inert g-ZnO monolayer sheet through introduction of dopant, facilitating its applications in the fields of catalysis and sensing. Furthermore, from this work we will gain usefull insights into the mechanism of Al-doped ZnO nanostructures sensing reducing gas, such as CO[45-48] and ethanol.[47, 49-51]

Acknowledgements:

This work was supported by the National Natural Science Foundation of China (Grant Nos. 11347186, and 51401078), the Henan Joint Funds of the National Natural Science Foundation of China (Grant No. U1404216), and the Science Fund of Educational Department of Henan Province of China (Grant No. 14A140015), and the Natural Science Foundation of Nanyang Normal University (No. ZX2014088, and QN2015020).

References:

1. K. Keis, L. Vayssieres, S.-E. Lindquist and A. Hagfeldt, *Nanostruct. Mater.*, 1999, **12**, 487-490.
2. S. Sakthivel, B. Neppolian, M. V. Shankar, B. Arabindoo, M. Palanichamy and V. Murugesan, *Sol. Energy Mater. Sol. Cells*, 2003, **77**, 65-82.
3. Z. Fan, D. Wang, P.-C. Chang, W.-Y. Tseng and J. G. Lu, *Appl. Phys. Lett.*, 2004, **85**, 5923-5925.
4. J. Goldberger, D. J. Sirbuly, M. Law and P. Yang, *J. Phys. Chem. B*, 2004, **109**, 9-14.
5. Q. H. Li, Y. X. Liang, Q. Wan and T. H. Wang, *Appl. Phys. Lett.*, 2004, **85**, 6389-6391.
6. Q. Wan, Q. H. Li, Y. J. Chen, T. H. Wang, X. L. He, J. P. Li and C. L. Lin, *Appl. Phys. Lett.*, 2004, **84**, 3654-3656.
7. A. B. Djurišić and Y. H. Leung, *Small*, 2006, **2**, 944-961.
8. M. H. Huang, S. Mao, H. Feick, H. Yan, Y. Wu, H. Kind, E. Weber, R. Russo and P. Yang, *Science*, 2001, **292**, 1897-1899.
9. C. H. Liu, J. A. Zapien, Y. Yao, X. M. Meng, C. S. Lee, S. S. Fan, Y. Lifshitz and S. T. Lee, *Adv. Mater.*, 2003, **15**, 838-841.
10. W. I. Park and G. C. Yi, *Adv. Mater.*, 2004, **16**, 87-90.
11. X. Wang, C. J. Summers and Z. L. Wang, *Nano Lett.*, 2004, **4**, 423-426.
12. C. Y. Jiang, X. W. Sun, G. Q. Lo, D. L. Kwong and J. X. Wang, *Appl. Phys. Lett.*, 2007, **90**, 263501.
13. V. Dhas, S. Muduli, W. Lee, S.-H. Han and S. Ogale, *Appl. Phys. Lett.*, 2008, **93**, 243108.
14. P. Gao and Z. L. Wang, *J. Phys. Chem. B*, 2002, **106**, 12653-12658.
15. H. Yan, J. Johnson, M. Law, R. He, K. Knutsen, J. R. McKinney, J. Pham, R. Saykally and P. Yang, *Adv. Mater.*, 2003, **15**, 1907-1911.
16. J.-J. Wu, S.-C. Liu, C.-T. Wu, K.-H. Chen and L.-C. Chen, *Appl. Phys. Lett.*, 2002, **81**, 1312-1314.
17. A. B. F. Martinson, J. W. Elam, J. T. Hupp and M. J. Pellin, *Nano Lett.*, 2007,

7, 2183-2187.

18. C. L. Freeman, F. Claeyssens, N. L. Allan and J. H. Harding, *Phys. Rev. Lett.*, 2006, **96**, 066102.
19. A. J. Kulkarni, M. Zhou, K. Sarasamak and S. Limpijumnong, *Phys. Rev. Lett.*, 2006, **97**, 105502.
20. C. Tusche, H. L. Meyerheim and J. Kirschner, *Phys. Rev. Lett.*, 2007, **99**, 026102.
21. X. Deng, K. Yao, K. Sun, W.-X. Li, J. Lee and C. Matranga, *J. Phys. Chem. C*, 2013, **117**, 11211-11218.
22. Y.-J. Zeng, K. Schouteden, M. N. Amini, S.-C. Ruan, Y.-F. Lu, Z.-Z. Ye, B. Partoens, D. Lamoen and C. Van Haesendonck, *ACS Appl. Mater. Interfaces*, 2015, **7**, 10617-10622.
23. M. Topsakal, S. Cahangirov, E. Bekaroglu and S. Ciraci, *Phys. Rev. B*, 2009, **80**, 235119.
24. T. M. Schmidt, R. H. Miwa and A. Fazzio, *Phys. Rev. B*, 2010, **81**, 195413.
25. Y. Wang, Y. Ding, J. Ni, S. Shi, C. Li and J. Shi, *Appl. Phys. Lett.*, 2010, **96**, 213117.
26. Q. Tang, Y. Li, Z. Zhou, Y. Chen and Z. Chen, *ACS Appl. Mater. Interfaces*, 2010, **2**, 2442-2447.
27. H. Guo, Y. Zhao, N. Lu, E. Kan, X. C. Zeng, X. Wu and J. Yang, *J. Phys. Chem. C*, 2012, **116**, 11336-11342.
28. Q. Chen, J. Wang, L. Zhu, S. Wang and F. Ding, *J. Chem. Phys.*, 2010, **132**, 204703.
29. E. Kan, K. Deng and F. Wu, *Nanoscale*, 2013, **5**, 12111-12114.
30. T. Kaewmaraya, A. De Sarkar, B. Sa, Z. Sun and R. Ahuja, *Comput. Mater. Sci.*, 2014, **91**, 38-42.
31. H. Behera and G. Mukhopadhyay, *Phys. Lett. A*, 2012, **376**, 3287-3289.
32. J. Ren, H. Zhang and X. Cheng, *Int. J. Quantum Chem.*, 2013, **113**, 2243-2250.
33. A. R. Botello-Méndez, F. López-Urías, M. Terrones and H. Terrones, *Nano*

Lett., 2008, **8**, 1562-1565.

34. A. Botello-Méndez, F. López-Urías, M. Terrones and H. Terrones, *Nano Res.*, 2008, **1**, 420-426.
35. L. Kou, C. Li, Z. Zhang and W. Guo, *ACS Nano*, 2010, **4**, 2124-2128.
36. Y.-H. Zhang, M.-L. Zhang, Y.-C. Zhou, J.-H. Zhao, S.-M. Fang and F. Li, *J. Mater. Chem. A*, 2014, **2**, 13129-13135.
37. S. Kouser, U. V. Waghmare and N. Tit, *Phys. Chem. Chem. Phys.*, 2014, **16**, 10719-10726.
38. N. Guo, R. Lu, S. Liu, G. W. Ho and C. Zhang, *J. Phys. Chem. C*, 2014, **118**, 21038-21041.
39. Y.-H. Lu, M. Zhou, C. Zhang and Y.-P. Feng, *J. Phys. Chem. C*, 2009, **113**, 20156-20160.
40. Y. Li, Z. Zhou, G. Yu, W. Chen and Z. Chen, *J. Phys. Chem. C*, 2010, **114**, 6250-6254.
41. E. H. Song, Z. Wen and Q. Jiang, *J. Phys. Chem. C*, 2011, **115**, 3678-3683.
42. M. Zhou, Y.-H. Lu, Y.-Q. Cai, C. Zhang and Y.-P. Feng, *Nanotechnology*, 2011, **22**, 385502.
43. S. Lin, X. Ye, R. S. Johnson and H. Guo, *J. Phys. Chem. C*, 2013, **117**, 17319-17326.
44. K. Mao, L. Li, W. Zhang, Y. Pei, X. C. Zeng, X. Wu and J. Yang, *Sci. Rep.*, 2014, **4**, 1-7.
45. J. F. Chang, H. H. Kuo, I. C. Leu and M. H. Hon, *Sens. Actuators, B*, 2002, **84**, 258-264.
46. S. Bai, T. Guo, Y. Zhao, R. Luo, D. Li, A. Chen and C. C. Liu, *J. Mater. Chem. A*, 2013, **1**, 11335-11342.
47. Y. Lingmin, F. Xinhui, C. Lei, Q. Lijun and Y. Wen, *Appl. Surf. Sci.*, 2013, **265**, 108-113.
48. M. Hjiri, L. El Mir, S. G. Leonardi, A. Pistone, L. Mavilia and G. Neri, *Sens. Actuators, B*, 2014, **196**, 413-420.
49. F. Paraguay D, M. Miki-Yoshida, J. Morales, J. Solis and W. Estrada L, *Thin*

Solid Films, 2000, **373**, 137-140.

50. Z. Yang, Y. Huang, G. Chen, Z. Guo, S. Cheng and S. Huang, *Sens. Actuators, B*, 2009, **140**, 549-556.
51. M. Zhao, X. Wang, J. Cheng, L. Zhang, J. Jia and X. Li, *Curr. Appl. Phys.*, 2013, **13**, 403-407.
52. H.-J. Freund, G. Meijer, M. Scheffler, R. Schlögl and M. Wolf, *Angew. Chem. Int. Ed.*, 2011, **50**, 10064-10094.
53. P. E. Blöchl, *Phys. Rev. B*, 1994, **50**, 17953-17979.
54. G. Kresse and J. Furthmüller, *Comput. Mater. Sci.*, 1996, **6**, 15-50.
55. G. Kresse and D. Joubert, *Phys. Rev. B*, 1999, **59**, 1758-1775.
56. J. P. Perdew, K. Burke and M. Ernzerhof, *Phys. Rev. Lett.*, 1996, **77**, 3865-3868.
57. H. J. Monkhorst and J. D. Pack, *Phys. Rev. B*, 1976, **13**, 5188-5192.
58. G. Henkelman, B. P. Uberuaga and H. Jonsson, *J. Chem. Phys.*, 2000, **113**, 9901-9904.
59. G. Henkelman, A. Arnaldsson and H. Jónsson, *Comput. Mater. Sci.*, 2006, **36**, 354-360.
60. P. A. Denis, R. Faccio and A. W. Mombru, *ChemPhysChem*, 2009, **10**, 715-722.
61. Y. Li, Z. Zhou, P. Shen and Z. Chen, *ACS Nano*, 2009, **3**, 1952-1958.
62. N. Mammen, S. Narasimhan and S. d. Gironcoli, *J. Am. Chem. Soc.*, 2011, **133**, 2801-2803.
63. P. Mars and D. W. Van Krevelen, *Chem. Eng. Sci.*, 1954, **3**, 41-59.
64. C. Doornkamp and V. Ponec, *J. Mol. Catal. A: Chem.*, 2000, **162**, 19-32.
65. V. Shapovalov and H. Metiu, *J. Catal.*, 2007, **245**, 205-214.
66. R. G. S. Pala, W. Tang, M. M. Sushchikh, J.-N. Park, A. J. Forman, G. Wu, A. Kleiman-Shwarsctein, J. Zhang, E. W. McFarland and H. Metiu, *J. Catal.*, 2009, **266**, 50-58.
67. E. W. McFarland and H. Metiu, *Chem. Rev.*, 2013, **113**, 4391-4427.
68. C. Zhang, P. Hu and A. Alavi, *J. Am. Chem. Soc.*, 1999, **121**, 7931-7932.

69. A. Bongiorno and U. Landman, *Phys. Rev. Lett.*, 2005, **95**, 106102.

70. C. Bürgel, N. M. Reilly, G. E. Johnson, R. Mitrić, M. L. Kimble, A. W. Castleman and V. Bonačić-Koutecký, *J. Am. Chem. Soc.*, 2008, **130**, 1694-1698.

71. D. Ma, Y. Tang, G. Yang, J. Zeng, C. He and Z. Lu, *Appl. Surf. Sci.*, 2015, **328**, 71-77.

72. A. Kokalj, *Corros. Sci.*, 2013, **68**, 195-203.

73. K. H. Warnick, B. Wang, D. E. Cliffel, D. W. Wright, R. F. Haglund and S. T. Pantelides, *Nano Lett.*, 2013, **13**, 798-802.

74. W. Wang, G. McCool, N. Kapur, G. Yuan, B. Shan, M. Nguyen, U. M. Graham, B. H. Davis, G. Jacobs, K. Cho and X. Hao, *Science*, 2012, **337**, 832-835.

75. Y.-G. Wang, D. Mei, V.-A. Glezakou, J. Li and R. Rousseau, *Nat. Commun.*, 2015, **6**, 1-8.

Table 1. The parameters for the adsorption of O_2 and CO molecules on the Al-g-ZnO monolayer sheet: adsorption energy (E_a), the nearest distance between the adsorbed molecules and the sheet (d), bond length of the adsorbed molecules ($d_{A\text{-}B}$). For Q, the values outside and inside the parenthesis are the amounts of charge gained by the adsorbed O_2 and donated by the doped Al atom, respectively. For M, the values outside and inside the parenthesis are the spin magnetic moments of the adsorbed molecules and the whole cell, respectively.

Adsorbate	E_a (eV)	Q (e)	M (μ_B)	d (Å)	$d_{A\text{-}B}$(Å)
O_2	2.30	-0.83 (-0.10)	0.98 (1.00)	1.90	1.39
CO	0.47	-0.37 (-0.07)	0.42 (0.49)	2.08	1.18

Figure captions:

Fig.1. (a) Atomic configurations of a 5×5 g-ZnO monolayer sheet. The O and Zn atoms of the sheet are represented by red and grey spheres, respectively, both of which are at the same plane. The position of the replaced Zn atom (the dopant Al atom) is marked with a blue circle. (b) The LDOS projected on the Zn 3d and 4s orbitals as well as the O 2p orbital. The position of the Fermi level (E_f) is indicated by a vertical dashed line. The positive and negative LDOS denote the spin-up and spin-down states, respectively.

Fig. 2. (a) Atomic configurations and electron density distributions (1.5×10^{-4} *e*/bohr^3) for the Al-g-ZnO monolayer sheet within the energy interval from -0.5 to 0 eV with respect to the Fermi level (E_f). (b) The upper panel shows the TDOS of the g-ZnO and Al-g-ZnO monolayer sheets, and the lower panel the LDOS of the doped Al atom.

Fig. 3. Atomic configurations of the four stable states for the adsorption of Al atoms on the pristine g-ZnO monolayer sheet. Note that the configuration shown in (d) contains the Al-g-ZnO monolayer sheet with a loosely bonded Zn atom, the transition of the configuration shown in (c) to which is barrierless.

Fig. 4. (a) The most stable configuration for the O_2 adsorption on the Al-g-ZnO monolayer sheet. (b) The TDOS for the configuration shown in (a) are shown in the upper panel, while the LDOS projected on the adsorbed O_2 and its bonded Zn and Al atoms in the lower panel. (c) The electron density distributions (2×10^{-3} *e*/bohr^3) for the configuration shown in (a) within the energy interval from -0.5 to 0 eV with respect to the Fermi level (E_f).

Fig. 5. (a) The most stable configuration for the CO adsorption on the Al-g-ZnO monolayer sheet. (b) The TDOS for the configuration shown in (a) are shown in the upper panel, while the LDOS projected on the adsorbed CO and its bonded Al atom in the lower panel.

Fig. 6. Atomic configurations and the relevant structural parameters (in Å) of the IS, TS1, MS1, MS2, TS2, and FS along the MEP for the CO oxidation on the Al-g-ZnO monolayer sheet. Both top and side views are displayed, as well as the energy change between neighboring states.

Fig. 7. The schematic energy profile corresponding to the states shown in Fig. (6). The reference energy is the sum of the total energies of the two free CO and one free O_2 molecules and the Al-g-ZnO monolayer sheet.

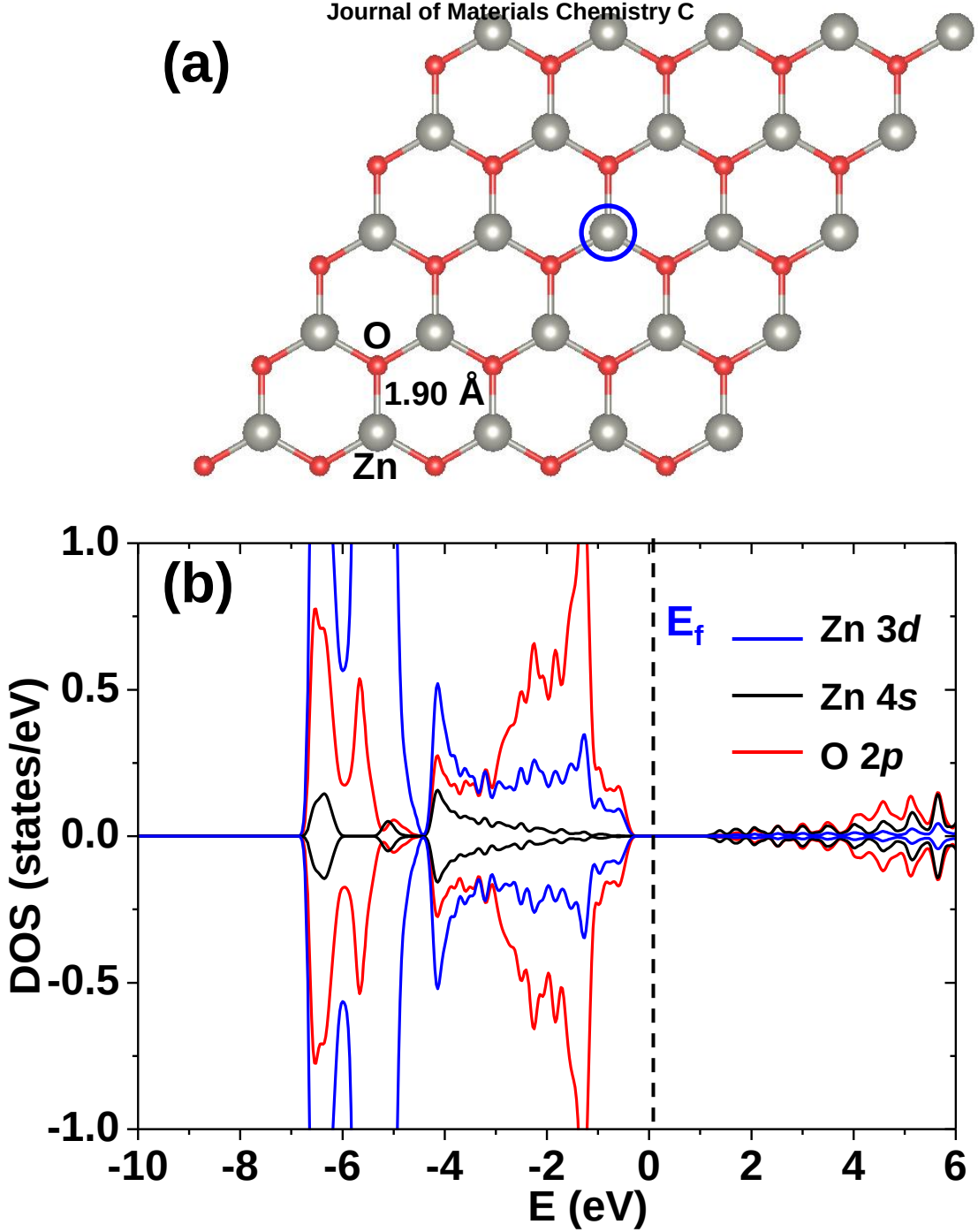

Fig. 1

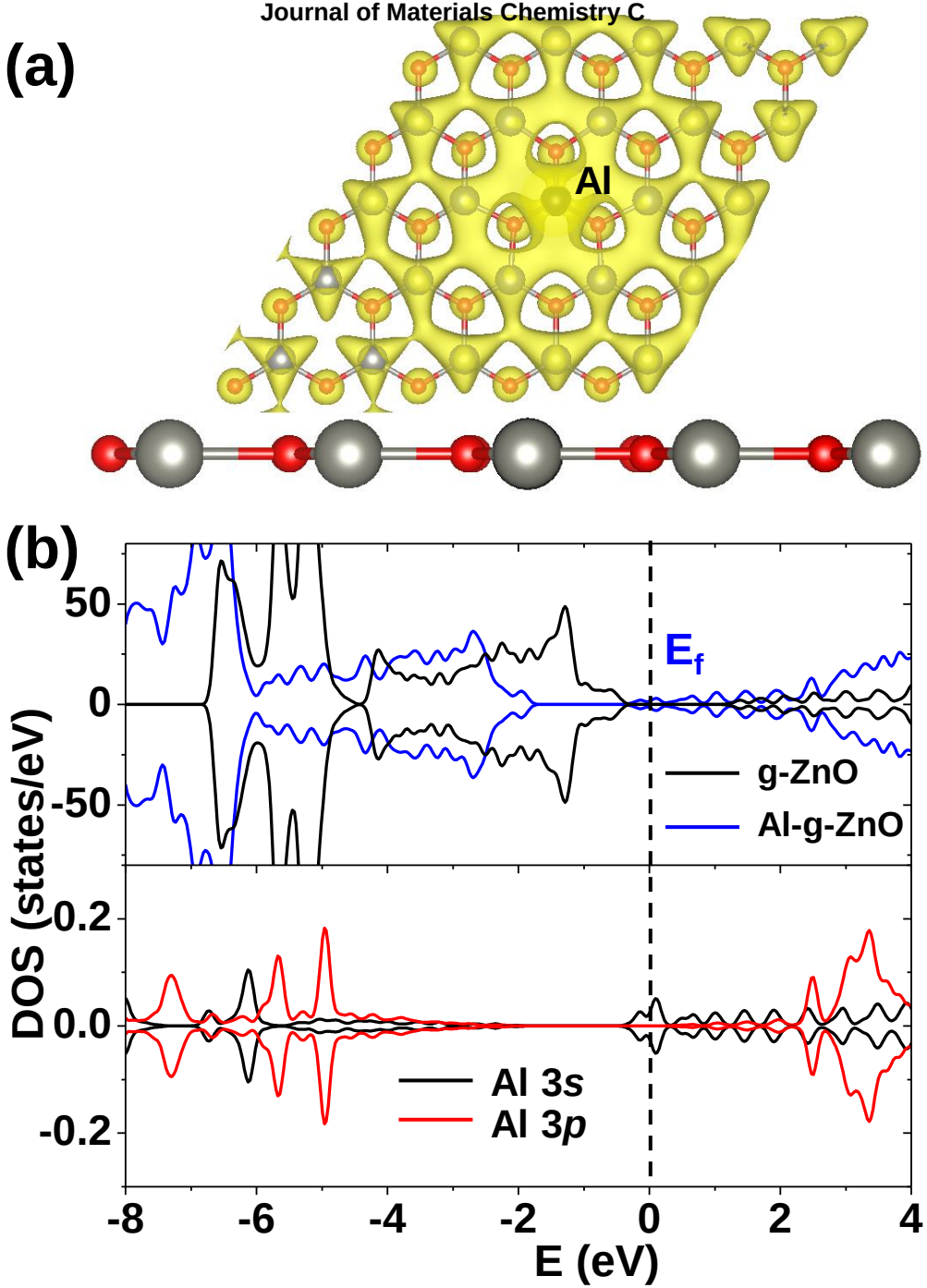

Fig. 2

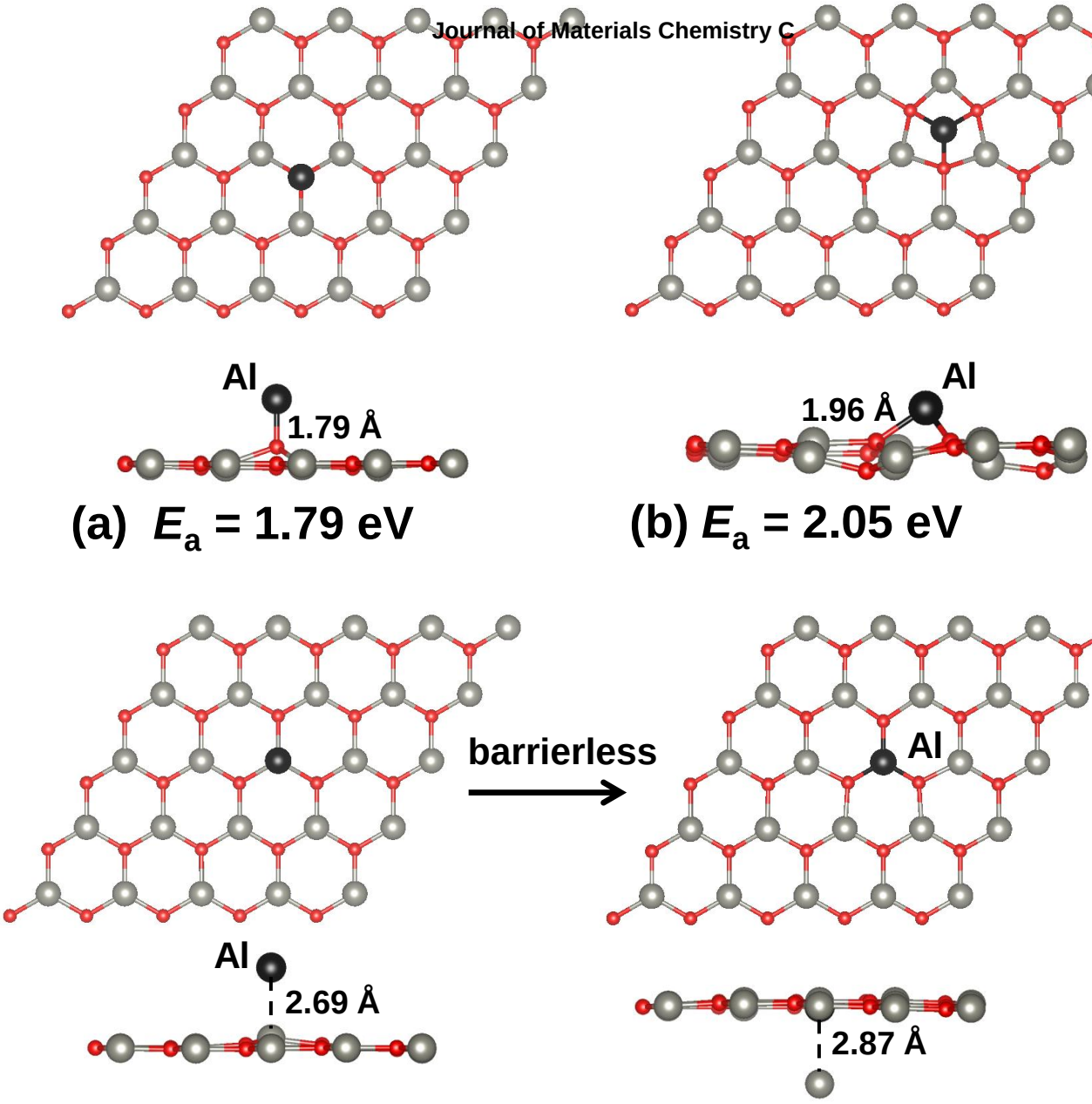

Fig. 3

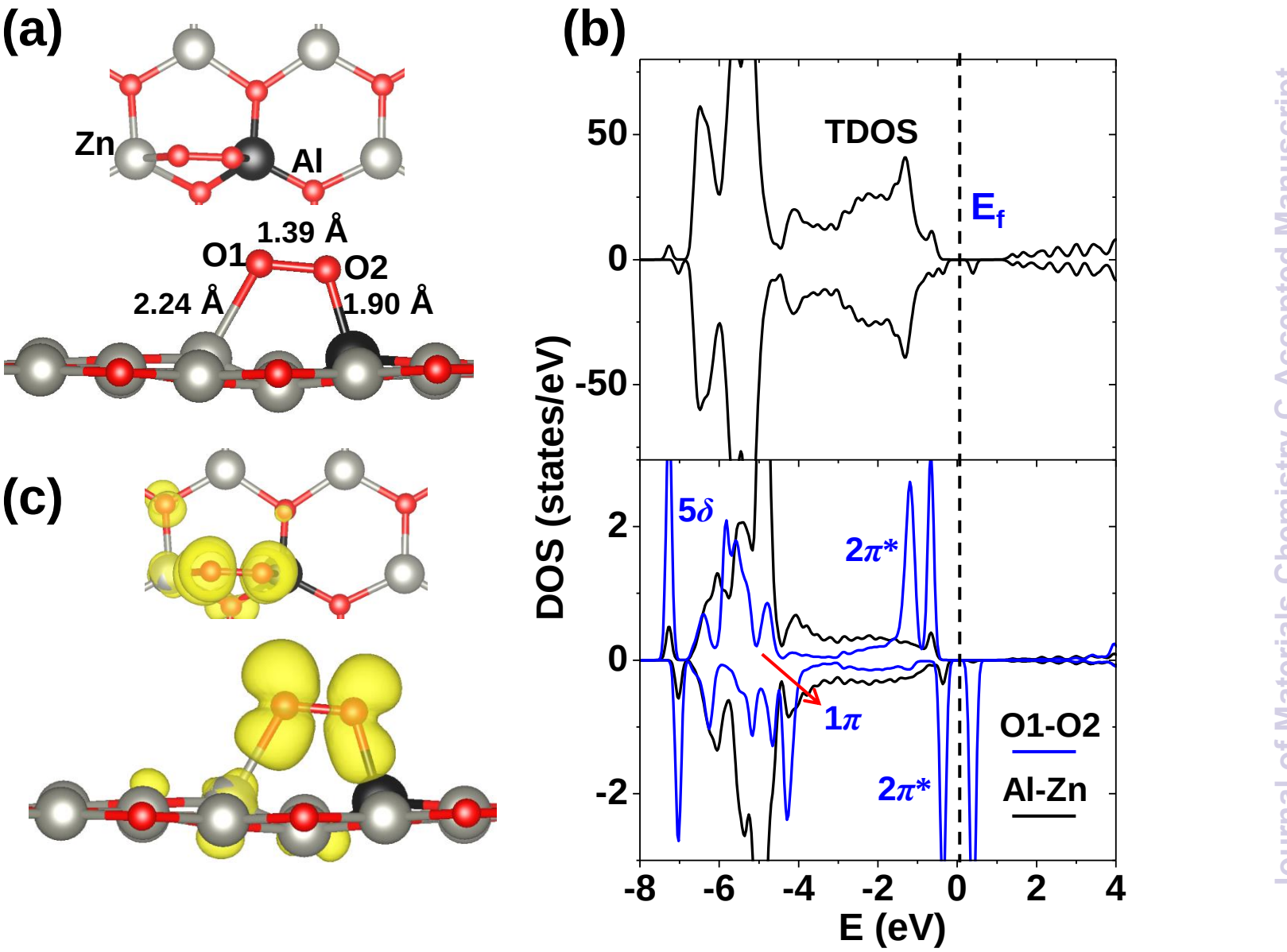

Fig. 4

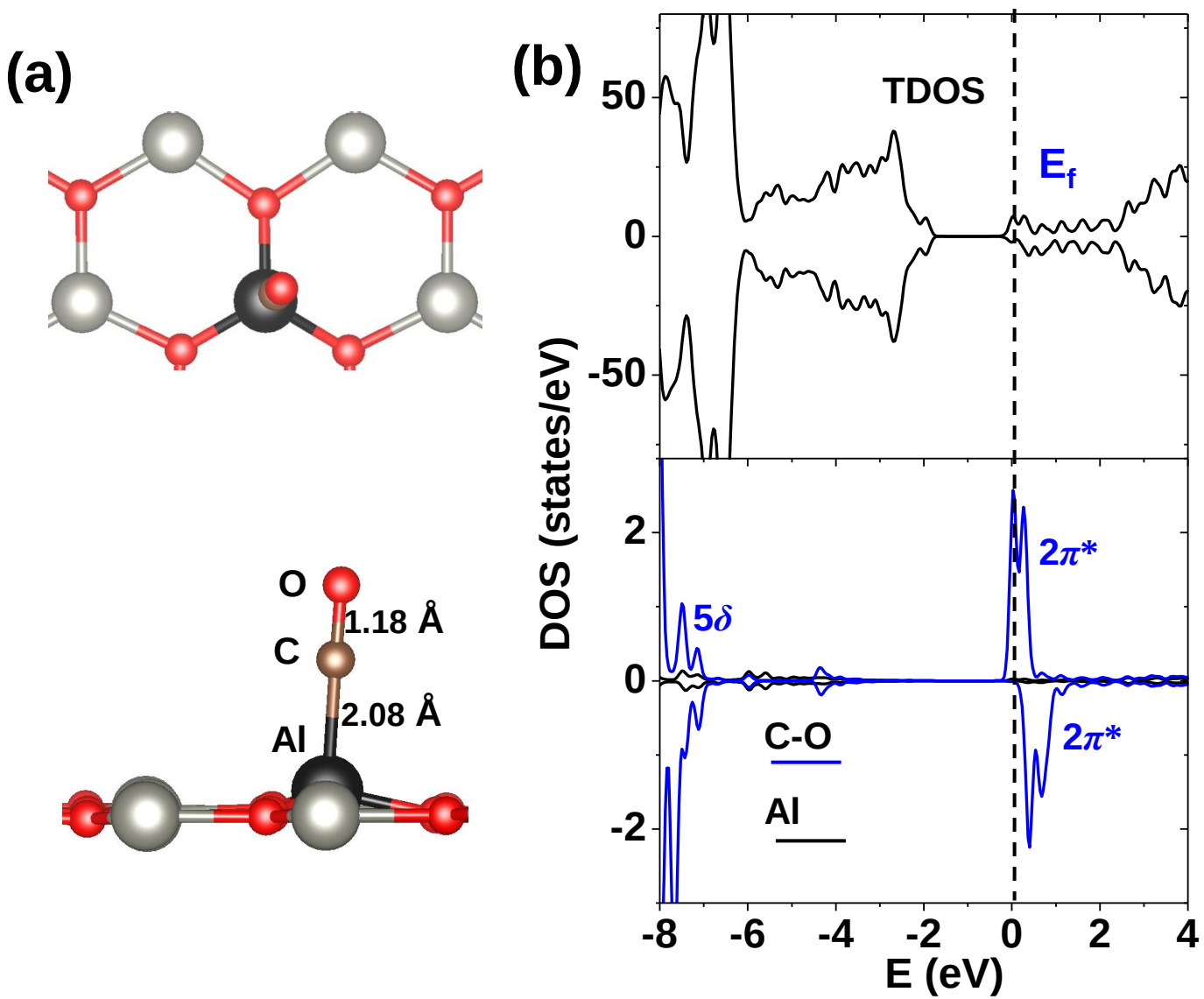

Fig. 5

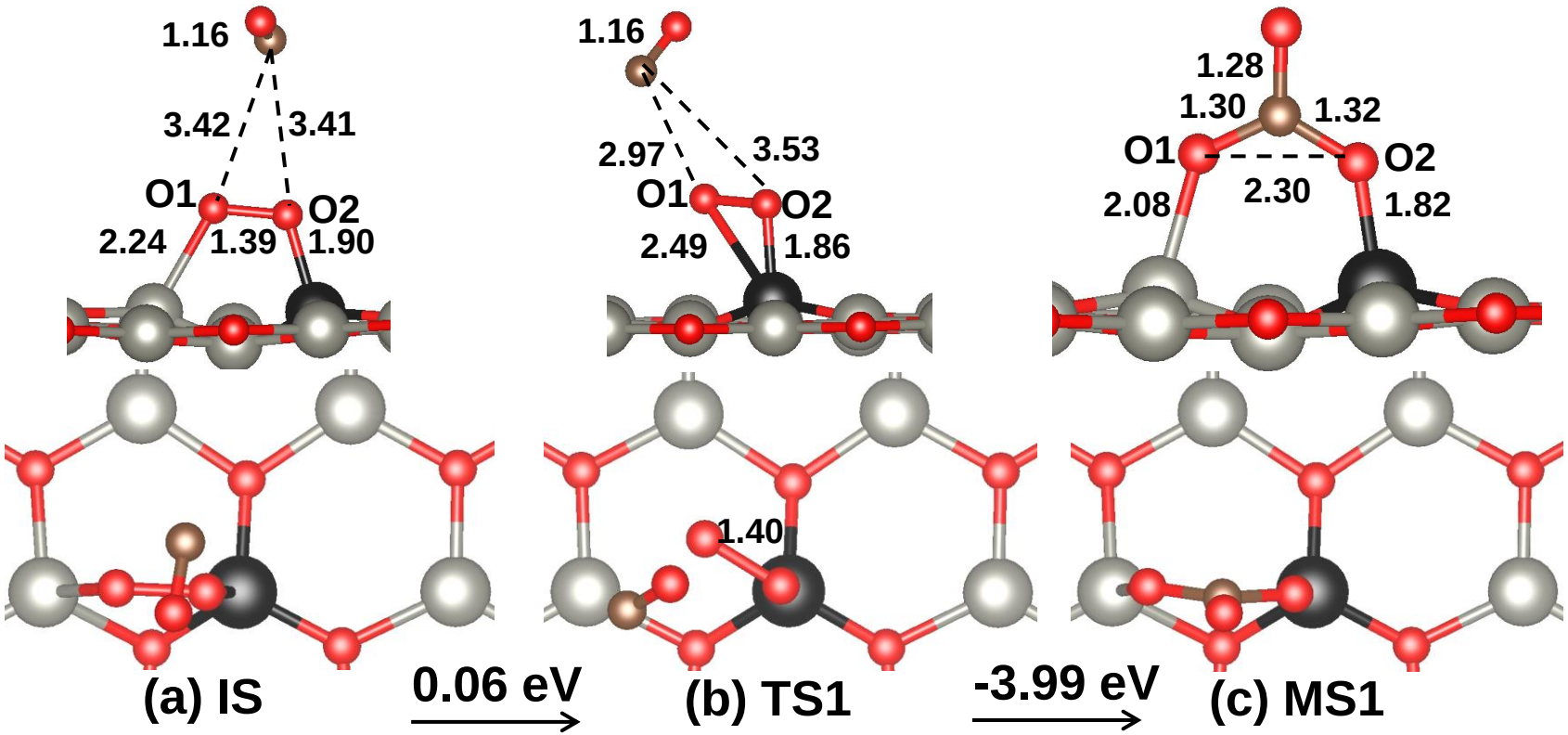

Fig. 6

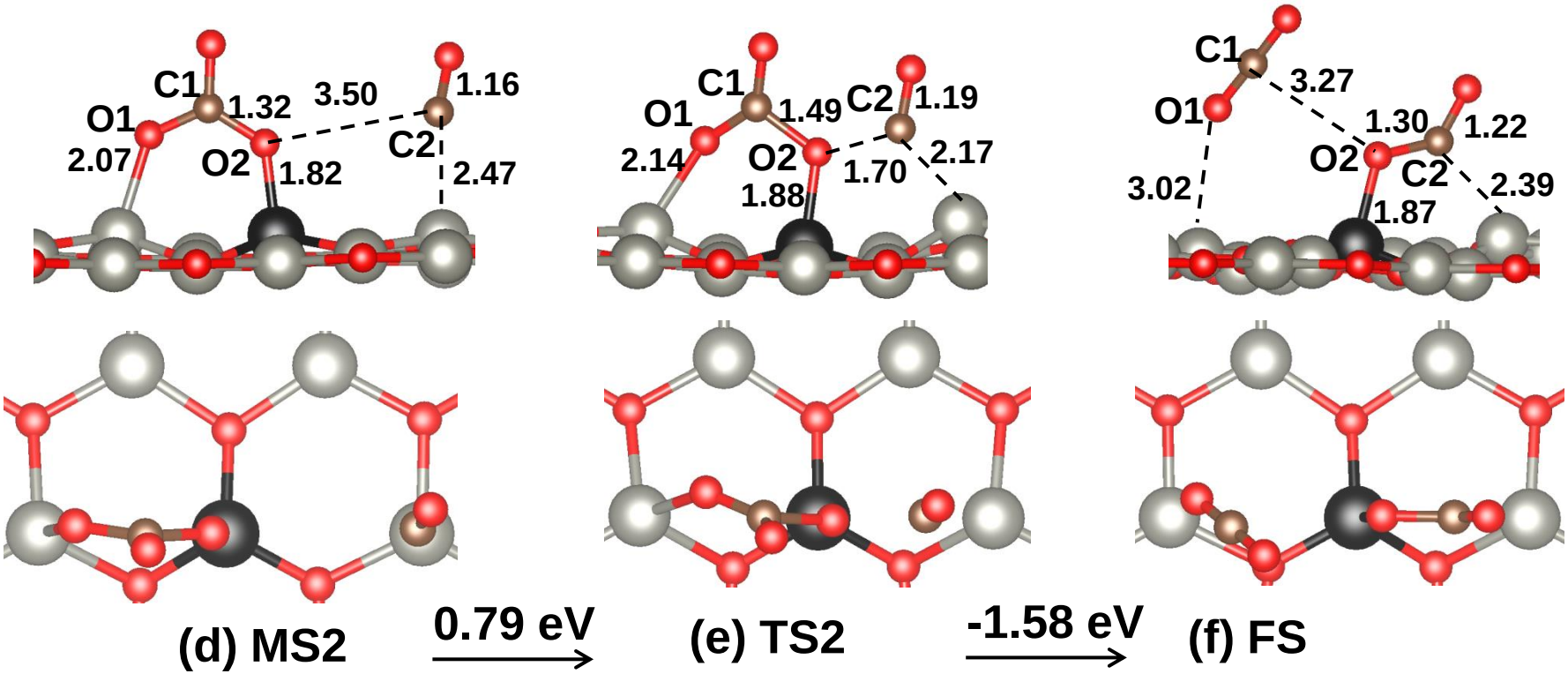

Fig. 6

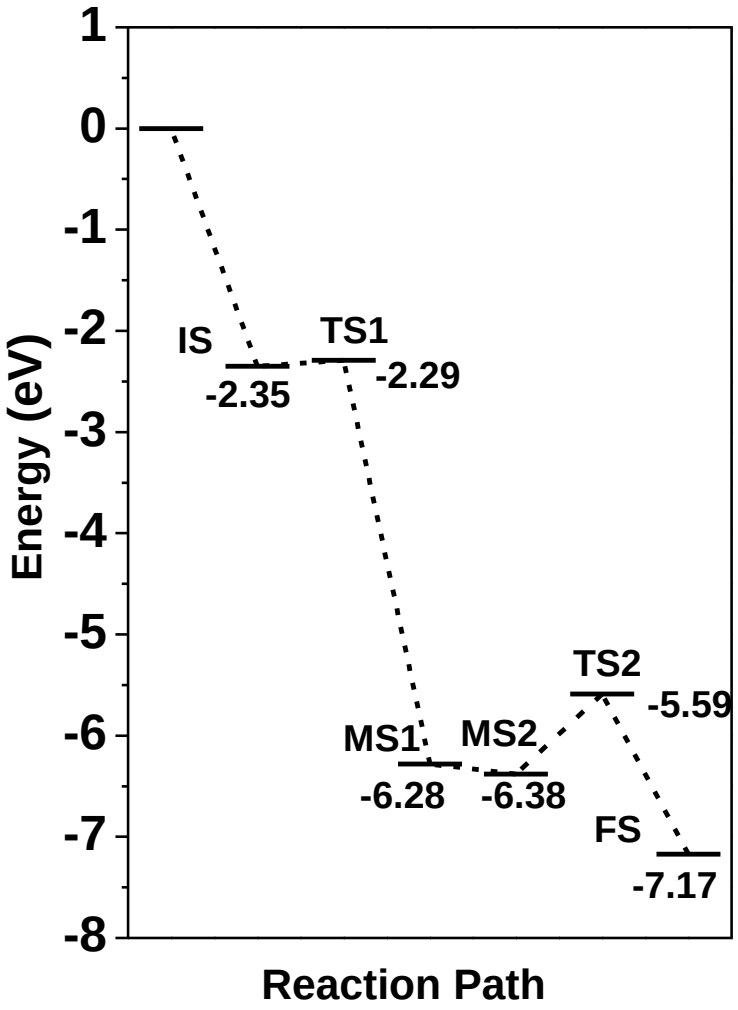

Fig. 7

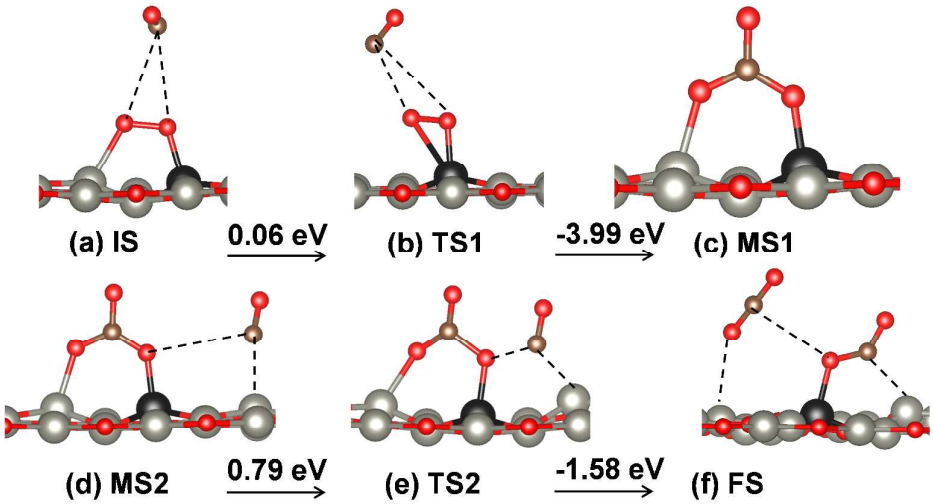

Three mechanisms for CO catalytic oxidation on Al-doped g-ZnO monolayer sheets were comparably studied, among which the Eley-Rideal mechanism is both energetically and dynamically more favorable.